Available online at www.sciencedirect.com
ScienceDirect
International Journal of Heat and Mass Transfer 50 (2007) 2260–2271
International Journal of HEAT and MASS TRANSFER
www.elsevier.com/locate/ijhmt

Conjugate natural convection around a finned pipe in a square enclosure with internal heat generation

Abdullatif Ben-Nakhi [a,*], Ali J. Chamkha [b]

[a] Mechanical Power and Refrigeration Department, College of Technological Studies, The Public Authority for Applied Education and Training, P.O. Box 42325, Shuweikh 70654, Kuwait
[b] Manufacturing Engineering Department, College of Technological Studies, The Public Authority for Applied Education and Training, P.O. Box 42325, Shuweikh 70654, Kuwait

Received 3 April 2006; received in revised form 18 September 2006
Available online 28 December 2006

Abstract

This work is focused on the numerical study of steady, laminar, conjugate natural convection around a finned pipe placed in the center of a square enclosure with uniform internal heat generation. Four perpendicular thin fins of arbitrary and equal dimensions are attached to the pipe whose internal surface is isothermally cooled. The sides of the enclosure are considered to have finite and equal thicknesses and their external sides are isothermally heated. The problem is put into dimensionless formulation and solved numerically by means of the finite-volume method. Representative results illustrating the effects of the finned pipe inclination angle and fins length on the streamlines and temperature contours within the enclosure are reported. In addition, results for the local and average Nusselt numbers are presented and discussed for various parametric conditions.

Keywords: Natural convection; Conjugate; Square enclosure; Thin fin; Internal heat generation; Finite volume

1. Introduction

During the last four decades, significant attention was given to the study of natural convection in enclosures subjected to simultaneous volumetric internal heat generation and external heating or cooling. This was due to the occurrence of natural convection in a wide range of application areas that include nuclear reactor design, post-accident heat removal in nuclear reactors, geophysics and underground storage of nuclear waste, energy storage systems and others.

Natural convection heat transfer in enclosures containing heat generating fluids with different geometrical parameters and boundary conditions has been extensively considered in the open literature. Steinberner and Reinke [1] performed experiments with a rectangular geometry and both upper and lower walls being cooled for Ra_I varying from 5×10^{10} to 3×10^{13}. Based on a numerical modeling effort, they developed correlations for the Nusselt number. Kulacki and Goldstein [2] experimentally measured heat transfer from a plane layer containing internal energy sources with equal boundary temperature. Lee and Goldstein [3] performed a laboratory experiment similar to that performed by Kulacki and Goldstein [2] but they employed an inclined square enclosure. Acharya and Goldstein [4] presented a numerical solution of natural convection in an externally heated square box of different aspect ratios and containing internal energy sources. Their study covered Ra_I from 10^4 to 10^7 and Ra_E from 10^3 to 10^6, and an enclosure inclination angle from 30° to 90°. They found that the flow pattern is related to the ratio Ra_E/Ra_I. Emara and Kulacki [5] reported a numerical study of thermal convection in a fluid layer driven by with uniform volumetric energy sources. The sides and lower surfaces of the rectangular domain were adiabatic walls

* Corresponding author. Present address: P.O. Box 3665, Salmiya 22037, Kuwait. Tel.: +965 972 2700; fax: +965 561 8866.
E-mail address: abdnakhi@yahoo.com (A. Ben-Nakhi).

0017-9310/$ - see front matter © 2006 Elsevier Ltd. All rights reserved.
doi:10.1016/j.ijheatmasstransfer.2006.10.036

Nomenclature

A	enclosure aspect ratio
d	internal diameter of the pipe (m)
D	dimensionless internal diameter of the pipe $= d/H$
g	gravitational acceleration (m/s^2)
Gr	Grashof number $= g\beta(T_h - T_c)H^3/\nu^2$
k	thermal conductivity (W/m K)
l	fin length (m)
L	dimensionless fin length $= l/H$
n	distance normal to s-axis (m)
N	dimensionless n-coordinate $= n/H$
Nu	local Nusselt number at solid–fluid interface
$\overline{Nu}$	average Nusselt number
p	fluid pressure (Pa)
P	dimensionless pressure of fluid $= \frac{p}{\rho}\left(\frac{H}{\alpha_f}\right)^2$
Pr	Prandtl number $= \nu/\alpha_f$
q	rate of internal heat generation per unit volume (W/m^3)
Ra_E	external Rayleigh number $= g\beta(T_h - T_c)H_3/(\alpha\nu)$
Ra_I	internal Rayleigh number $= g\beta qH^5/(\alpha\nu k)$
Ra_{EI}	external to internal Raleigh numbers ratio $= Ra_E/Ra_I$
s	coordinate adopted for distance along solid–fluid interfaces (m)
S	dimensionless s-coordinate $= s/H$
T	temperature (K)
u	x-component of velocity (m/s)
U	dimensionless X-component of velocity $= uH/\alpha_f$
v	y-component of velocity (m/s)
V	dimensionless Y-component of velocity $= vH/\alpha_f$
w	thickness of solid item (m)
x	horizontal distance (m)
X	dimensionless horizontal distance $= x/H$
y	vertical distance (m)
Y	dimensionless vertical distance $= y/H$
z	total length of the interface between the fluid and the finned pipe (m)
Z	dimensionless $z = z/H$

Greek symbols

ε	thin fin inclination angle (°)
α	thermal diffusivity (m^2/s)
β	thermal expansion coefficient (1/K)
κ	solid-to-fluid thermal conductivity ratio $= k_s/k_f$
ν	kinematic viscosity (m^2/s)
θ	dimensionless temperature $= (T - T_c)/(T_h - T_c)$
ρ	density (kg/m^3)
ω	dimensionless thickness of solid item $= w/H$
Ψ	stream function (m^2/s)
ψ	dimensionless stream function $= \Psi/\alpha_f$
∇^2	Laplacian operator

Subscripts

c	cold surface
e	enclosure wall
f	fluid
fin	fin
fp	finned pipe
h	heated surface
in	internal surface of the pipe
p	pipe
s	solid

and the upper surface was either rigid or free isothermal boundary. Rahman and Sharif [6] conducted a numerical investigation for free convective laminar flow of a fluid with or without internal heat generation ($Ra_E = Ra_I = 2 \times 10^5$) in rectangular enclosures of different aspect ratios (from 0.25 to 4), at various angles of inclination, of insulated side walls, heated bottom, and cooled top walls. They observed that for $Ra_E/Ra_I > 1$, the convective flow and heat transfer was almost the same as that in a cavity without internal heat generating fluid. Kawara et al. [7] experimentally studied natural convection in a differentially heated vertical fluid layer of $Pr = 5.85$ with internal heating. Fusegi et al. [8] reported a numerical study on natural convection in square cavity with uniform internal heat generation and differentially heated vertical sidewalls. Fusegi et al. [9] also generated results for the same problem but for a rectangular cavity of different aspect ratios. Fusegi et al. studies [8,9] involved high external and internal Rayleigh numbers as $Ra_E = 5 \times 10^7$ and Ra_I varied from 10^9 to 10^{10}. Their results agreed with the experimental results of Kawara et al. [7]. Oztop and Bilgen [10] numerically studied a differentially heated, partitioned, square cavity containing a heat generating fluid. The vertical walls were isothermal while the horizontal walls were adiabatic and an isothermal cold partition was attached to the bottom wall. The external and internal Rayleigh numbers (i.e. Ra_E and Ra_I) ranged from 10^3 to 10^6. They observed two distinct flow regimes based on on the ratio Ra_E/Ra_I. Shim and Hyun [11] presented the time-dependent behavior of natural convection in a differentially heated square cavity due to impulsively switched on uniform internal heat generation. They concluded that the transient behavior is dependent on Ra_I/Ra_E and based on its value, three flow stages were distinguished. Baytas [12] investigated the effect of the uniformly distributed sinusoidal heat source generation on the fluid flow and heat transfer within a two-dimensional square cavity. Liaqat and Baytas [13] studied conjugate natural convection in a square enclosure containing uniform volumetric sources and having thick conducting walls. They illustrated the importance of performing conjugate investigations instead of conventional non-conjugate analyses.

The purpose of the present work is to study conjugate natural convection inside a square enclosure with uniform internal heat generation and having a finned pipe in its center. The enclosure walls are assumed to be uniformly conductive of equal thicknesses and their external sides are isothermally heated. The finned pipe has four perpendicular fins of uniform thickness and conductivity, and its internal surface is cooled isothermally. The effects of finned pipe orientation and fins length on the flow and heat transfer characteristics are studied.

2. Mathematical model

Consider steady laminar, two-dimensional, conjugate natural convection with uniform internal heat generation around a motionless finned pipe placed in the center of a square enclosure bounded by uniform thick walls, as shown in Fig. 1. The internal surface of the pipe is isothermally cooled and maintained at a temperature T_c while the external surface of the thick walls is kept at a uniform hot temperature T_h. The bounded fluid is assumed to be incompressible, viscous, and Newtonian having constant thermophysical properties. The effect of viscous dissipation and radiation heat transfer are negligible. The acceleration due to gravity acts in the vertical downward direction. It will be further assumed that the temperature differences in the domain under consideration is small enough to justify the employment of the Boussinesq approximation and the neglect of the radiation effects. It is worth noting that the depth of the current geometry is long enough so that a two-dimensional assumption is justified.

The governing equations for this problem are based on the balance laws of mass, linear momentum and energy. Although the current study is concerned with the steady state behavior, the transient mathematical model is employed in order to overcome the instabilities associated with internal heat generation. Taking into account the assumptions mentioned above, and applying the Boussinesq approximation for the body force terms in the momentum equations, the governing equations for the fluid region of the domain can be written in dimensionless formulation as:

$$\frac{\partial U}{\partial X}+\frac{\partial V}{\partial Y}=0 \tag{1}$$

$$\frac{\partial U}{\partial \tau}+U\frac{\partial U}{\partial X}+V\frac{\partial U}{\partial Y}=-\frac{\partial P}{\partial X}+Pr\left(\frac{\partial^2 U}{\partial X^2}+\frac{\partial^2 U}{\partial Y^2}\right) \tag{2}$$

$$\frac{\partial V}{\partial \tau}+U\frac{\partial V}{\partial X}+V\frac{\partial V}{\partial Y}=-\frac{\partial P}{\partial Y}+Pr\left(\frac{\partial^2 V}{\partial X^2}+\frac{\partial^2 V}{\partial Y^2}\right)+\frac{Ra_E}{Pr}\theta \tag{3}$$

$$\frac{\partial \theta}{\partial \tau}+U\frac{\partial \theta}{\partial X}+V\frac{\partial \theta}{\partial Y}=\left(\frac{\partial^2 \theta}{\partial X^2}+\frac{\partial^2 \theta}{\partial Y^2}\right)+\frac{Ra_I}{Ra_E Pr} \tag{4}$$

For the solid regions,

$$\frac{\partial \theta}{\partial \tau}=\nabla^2\theta \tag{5}$$

In writing Eqs. (1)–(5), the following dimensionless parameters and definitions are used.

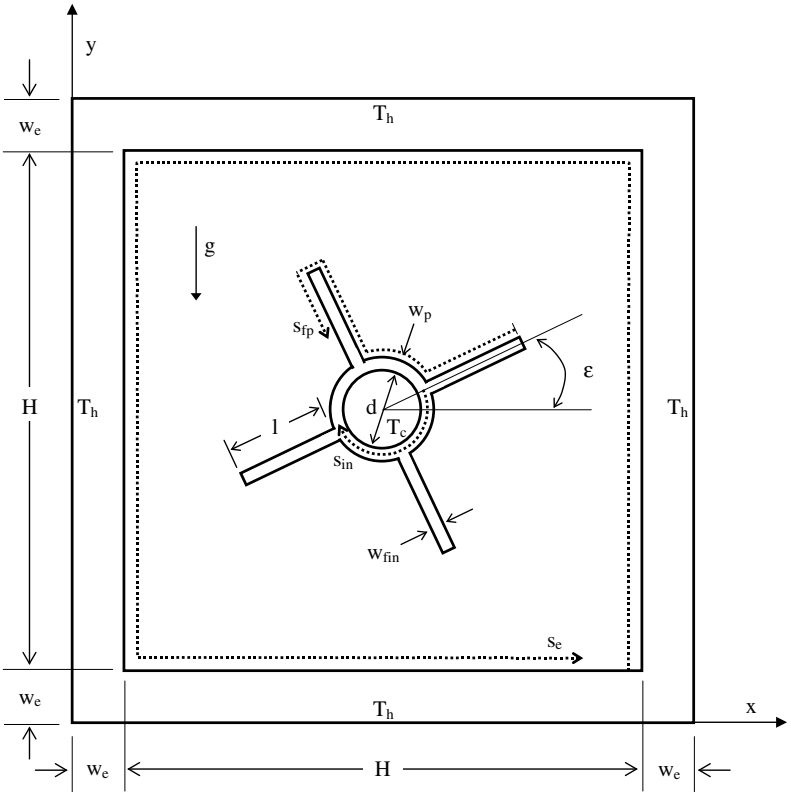

Fig. 1. Schematic diagram and coordinate system for a square enclosure with inclined finned pipe at the center of the cavity.

$$X=\frac{x}{H},\quad Y=\frac{y}{H},\quad \tau=\frac{\alpha t}{H^2},\quad U=u\frac{H}{\alpha}$$
$$V=v\frac{H}{\alpha},\quad Pr=\frac{v}{\alpha},\quad \theta=\frac{(T-T_c)}{(T_h-T_c)}$$
$$Ra_E=\frac{g\beta(T_h-T_c)H^3}{\alpha v},\quad Ra_I=\frac{g\beta qH^5}{\alpha vk} \tag{6}$$

where the dimensionless parameters appearing in the above equations are given in the Nomenclature list.

Motionless fluid (i.e. $U=V=0$), $P=0$, and cold isothermal state (i.e. $\theta=0$) are assumed as initial condition (i.e. $\tau=0$). The physical boundary conditions can be written as

at all solid–fluid interfaces $U=V=0$ (7a)

in the solid regions $U=V=P=0$ (7b)

at finned pipe–fluid interface $\dfrac{\partial\theta_f}{\partial N_{fp}}=\kappa_{fp}\left(\dfrac{\partial\theta_{fp}}{\partial N_{fp}}\right)$ (7c)

at internal surface of the pipe $\theta=0$ (7d)

$X=0$ or $1+2\omega_e$ $\theta=1$ (7e)

$X=\omega_e$ or $1+\omega_e$, $\omega_e<Y<1+\omega_e$ $\left(\dfrac{\partial\theta}{\partial X}\right)_f=\kappa_e\left(\dfrac{\partial\theta}{\partial X}\right)_e$ (7f)

$Y=0$ or $1+2\omega_e$ $\theta=1$ (7g)

$Y=\omega_e$ or $1+\omega_e$, $\omega_e<X<1+\omega_e$ $\left(\dfrac{\partial\theta}{\partial Y}\right)_f=\kappa_e\left(\dfrac{\partial\theta}{\partial Y}\right)_e$ (7h)

The stream function can be defined in the usual way as

$$v=-\frac{\partial\Psi}{\partial x},\quad u=\frac{\partial\Psi}{\partial y} \tag{8a}$$
$$\psi=\frac{\Psi}{\alpha_f} \tag{8b}$$

The local Nusselt number for the solid–fluid interfaces is given by:

$$Nu_e=\left(\frac{\partial\theta}{\partial N_e}\right)_{N_e=0} \tag{9a}$$
$$Nu_{fp}=\left(\frac{\partial\theta}{\partial N_{fp}}\right)_{N_{fp}=0} \tag{9b}$$

The average Nusselt number at the three boundaries is examined in the current study, two of which are internal and one is external with respect to the computation domain. The two internal boundaries are the enclosure wall–cavity interface and the finned pipe–cavity interface. The average Nusselt number for the former boundary is $\overline{Nu}_e$ and $\overline{Nu}_{fp}$ is for the latter boundary. The third boundary is at the internal surface of the finned pipe, for which average Nusselt number is $\overline{Nu}_{in}$. The three average Nusselt numbers are given by:

$$\overline{Nu}_e=\frac{1}{4}\int_0^4\left(\frac{\partial\theta}{\partial N_e}\right)_{N_e=0}dS_e \tag{10a}$$

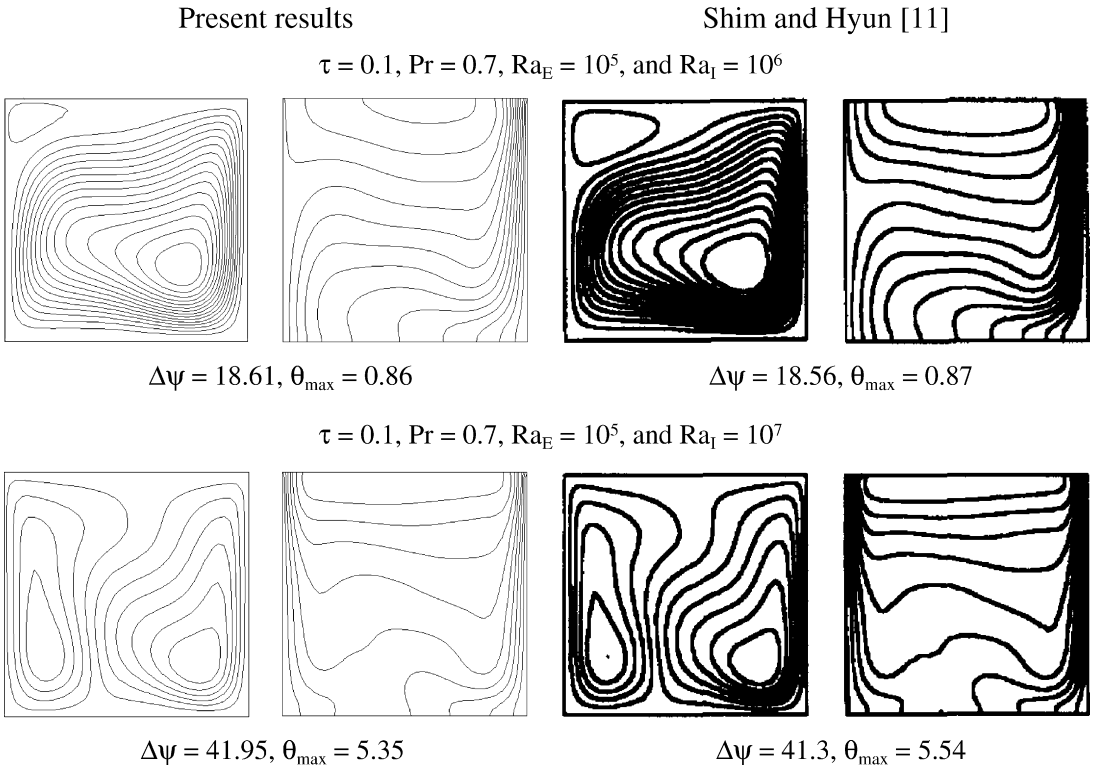

Fig. 2. Comparison of stream functions and isotherms with those of Shim and Hyun [11].

$$\overline{Nu}_{\mathrm{fp}} = \frac{1}{Z}\int_0^Z \left(\frac{\partial\theta}{\partial N_{\mathrm{fp}}}\right)_{N_{\mathrm{fp}}=0} \mathrm{d}S_{\mathrm{fp}},$$

$$Z = \frac{2\pi\left(w_{\mathrm{p}} + \frac{d}{2}\right)}{H} + 8L \tag{10b}$$

$$\overline{Nu}_{\mathrm{in}} = \frac{1}{\pi D}\int_0^{\pi D} \left(\frac{\partial\theta}{\partial N_{\mathrm{in}}}\right)_{N_{\mathrm{in}}=0} \mathrm{d}S_{\mathrm{in}} \tag{10c}$$

where $S = s/H$ and s is coordinate adopted for distance along solid–fluid interfaces. As shown in Fig. 1 s_{e} and s_{fp} advance counter clockwise, while s_{in} proceeds clockwise. $N = n/H$ where n is the distance locally normal to s-axis. These coordinates are defined in such a way to produce positive Nu when the fluid inside the cavity is losing heat.

3. Numerical algorithm

The governing Eqs. (1)–(5) for steady, laminar, two-dimensional conjugate natural convection heat transfer in a square enclosure subjected to its corresponding boundary conditions Eqs. (7a)–(7h) are solved using the Gauss–Seidel point-by-point method as discussed by Patankar [14] along with under-relaxation factors for θ, U, V, and P. The pressure-velocity coupling is resolved using the SIMPLEC algorithm [15]. The convective terms were approximated by the second-order upwind discretization scheme and the diffusive terms with the central differencing scheme. The convergence criterion employed was the standard relative error, which is based on the maximum norm given by

$$\Delta = \max\left\{\frac{\|\theta^m - \theta^{m-1}\|_\infty}{\|\theta^m\|_\infty}, \frac{\|U^m - U^{m-1}\|_\infty}{\|U^m\|_\infty}, \frac{\|V^m - V^{m-1}\|_\infty}{\|V^m\|_\infty}, \frac{\|P^m - P^{m-1}\|_\infty}{\|P^m\|_\infty}\right\} \leqslant 10^{-8} \tag{11}$$

where the operator $\|\eta\|_\infty$ indicates the maximum absolute value of the variable over all the grid points in the computational domain, and m and $m-1$ represent the current and previous iterations, respectively.

An unstructured grid of tri-angular mesh elements was employed in the current work. Approximately of 14,500 nodes were used in the model as the total number of nodes used depends on the fin length and inclination angle. The Aspect Ratio and Skewness of the mesh cells have significant

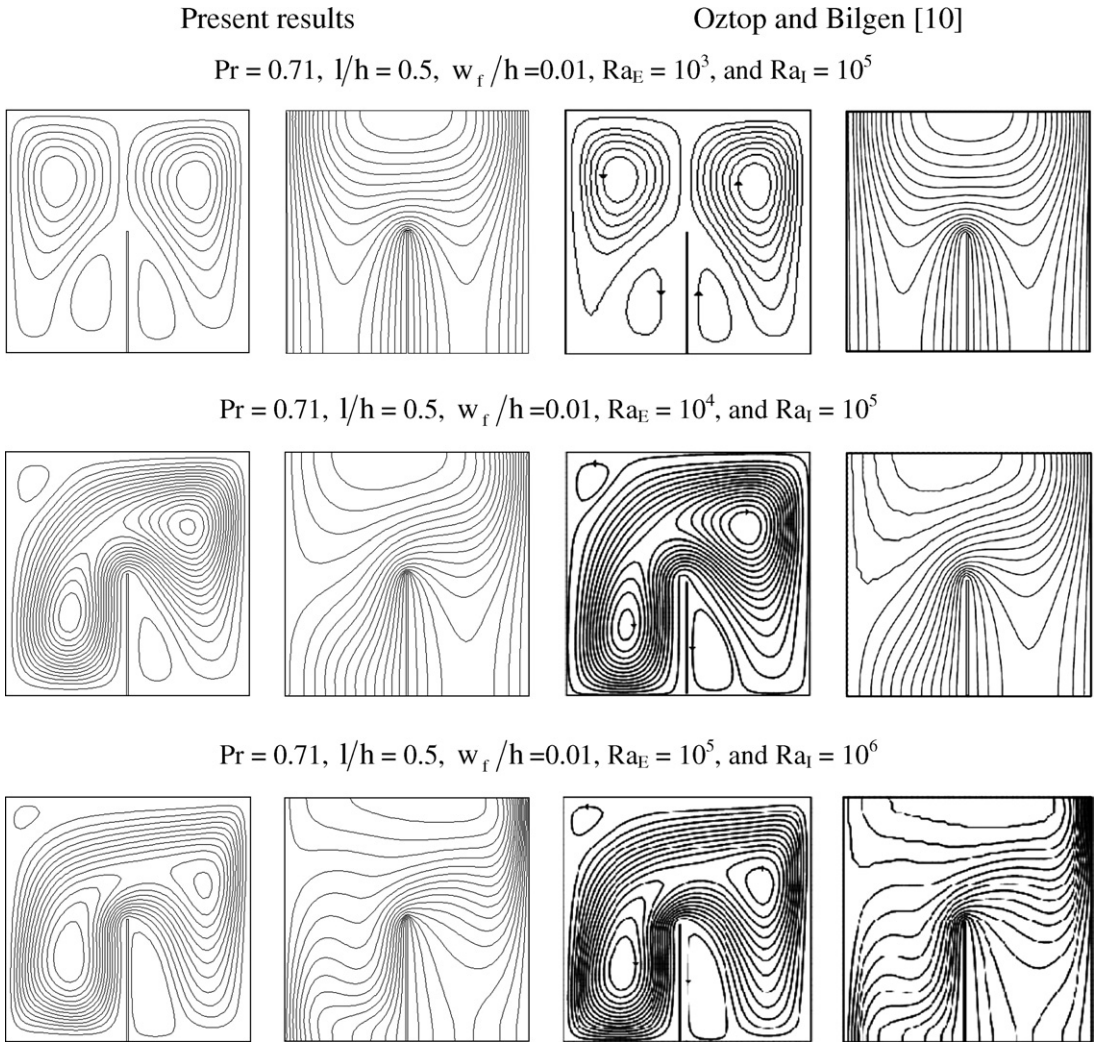

Fig. 3. Comparison of stream functions and isotherms with those of Oztop and Bilgen [10].

impact on the accuracy of the numerical solution. In the current work, the mesh quality of the numerical model was analyzed by means of Aspect Ratio, EquiAngle Skew, and Equisize Skew of each cell within the domain. The aspect ratio is defined by

$$Q_{\mathrm{AR}} = 0.5\frac{R}{r} \geqslant 1.0 \tag{12}$$

where r and R represent the radii of the circles that inscribe and circumscribe, respectively, the mesh element. For the range of fin lengths and inclination angles employed in the current study, about 96% of the cells have $1.0 \leqslant Q_{\mathrm{AR}} \leqslant 1.09$ where $Q_{\mathrm{AR}} = 1.0$ describes an equilateral element.

The EquiAngle Skew is a normalized measure of skewness that is defined as follows:

$$Q_{\mathrm{EAS}} = \max\left\{\frac{\Phi_{\max} - 60}{120}, \frac{60 - \Phi_{\min}}{60}\right\} \tag{13}$$

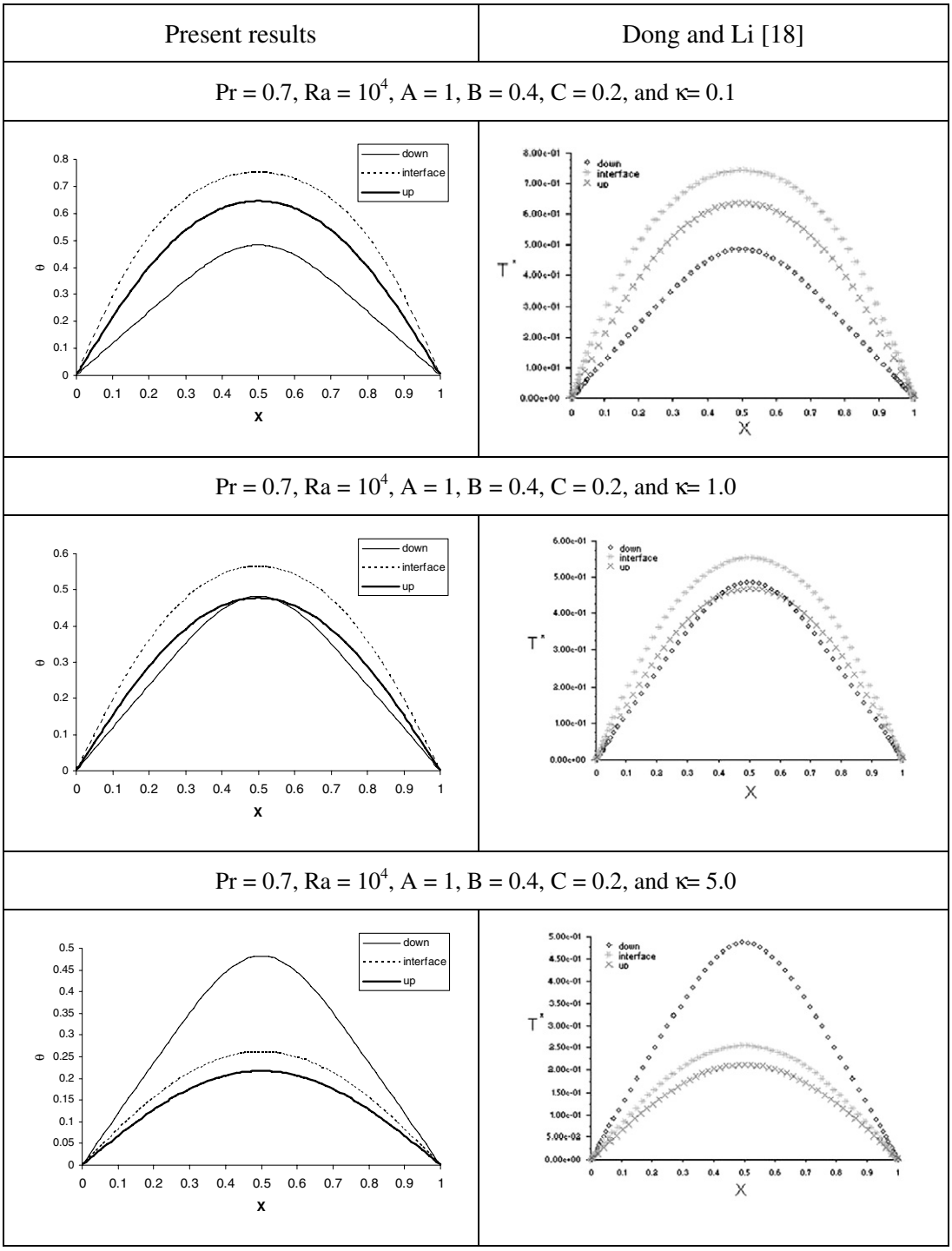

Fig. 4. Comparison of dimensionless temperature distribution with those of Dong and Li [18].

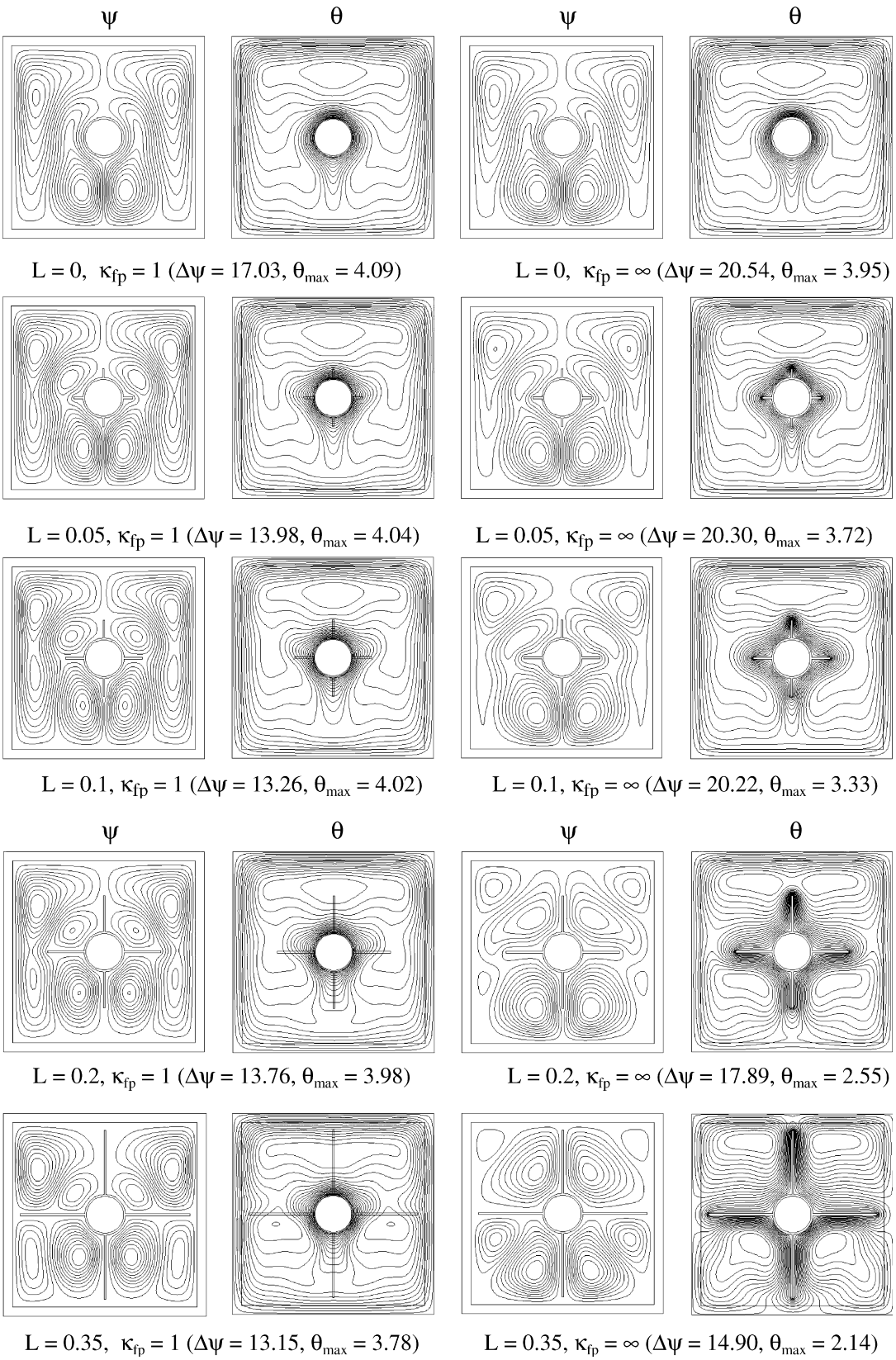

Fig. 5. Effects of L and κ_{fp} on the contour maps of the streamlines and isotherms for $\varepsilon = 0$, $Ra_E = 10^5$, and $Ra_I = 10^7$.

where Φ_{max} and Φ_{min} are the maximum and minimum angles (in degrees) between the edges of the triangular cell. Accordingly, $0.0 \leqslant Q_{EAS} \leqslant 1.0$ where $Q_{EAS} = 0.0$ describes an equilateral element, and $Q_{EAS} = 1.0$ describes

a completely degenerate (poorly shaped) element. Around 90% of the cells have $0.0 \leqslant Q_{EAS} \leqslant 0.13$ and 96% of the cells have $0.0 \leqslant Q_{EAS} \leqslant 0.24$. In general, high-quality meshes contain elements that possess Q_{EAS} values not exceeding 0.25. The EquiSize Skew (Q_{ESS}) is a measure of skewness that is defined as follows:

$$Q_{ESS} = \frac{\xi_{eq} - \xi^*}{\xi_{eq}} \tag{14}$$

where ξ^* is the area of the triangular cell, and ξ_{eq} is the maximum area of an equilateral triangular cell the circumscribing radius of which is identical to that of the mesh element. Accordingly, $0.0 \leqslant Q_{ESS} \leqslant 1.0$ where $Q_{ESS} = 0.0$ describes an equilateral element, and $Q_{ESS} = 1.0$ describes a completely degenerate (poorly shaped) element. Above 80% of the cells have $0.0 \leqslant Q_{EAS} \leqslant 0.01$ and around 96% of the cells have $0.0 \leqslant Q_{AR} \leqslant 0.1$. In general, high-quality meshes contain elements Q_{ESS} values of 0.1 or less. In the present work, all requirements for high quality meshes are satisfied.

In order to reduce round-off errors, double precision computation was employed. The accuracy of the numerical scheme is validated by means of several inter-model comparisons. First, the average Nusselt number $\overline{Nu}$ obtained by the adopted numerical scheme for a differentially-heated square enclosure consisting of three thin sides and one thick vertical wall under various Grashof numbers was compared against those reported by Kaminski and Prakash [16] and Liaqat and Baytas [13], The results were exactly similar for most of the cases and the maximum deviation from the results reported by Kaminski and Prakash [16], and Liaqat and Baytas [13] were 1.25% and 0.7%, respectively. The detailed results are reported by Ben-Nakhi and Chamkha [17]. The second validation test is performed by a comparison against the results presented by Shim and Hyun [11] who considered transient natural convection in square cavity with internal heat generation. Good agreement was achieved as can be seen from the streamline and temperature contours and extreme values in Fig. 2 for $\tau = 0.1$, $Pr = 0.7$, $Ra_E = 10^5$, and $Ra_I = 10^6$ and 10^7. In the third validation test, acceptable conformity was attained when the contour maps of the streamlines and isotherms for some of the cases reported by Oztop and Bilgen [10] were regenerated as shown in Fig. 3 for $Pr = 0.71$, $l/h = 0.5$, $w_f/h = 0.01$, and three combinations of Ra_E and Ra_I. The fourth verification practice was performed against results for comparable geometry produced by Dong and Li [18], who considered conjugate natural convection around a pipe centered in a square enclosure. Excellent agreement was achieved for $Pr = 0.7$, $Ra = 10^4$, $A = 1$, $D = 0.4$, $\omega = 0.2$, and $\kappa = 0.1$, 1.0, and 5.0. Due to space limitation only dimensionless temperature distribution along three boundaries are presented in Fig. 4. These various favorable comparisons lend confidence in the numerical results to be presented in the next section.

4. Results and discussion

In this section, numerical results for the streamline and temperature contours for various values of the fin inclination angle ε, fin dimensionless length L, solid-to-fluid thermal conductivity ratio κ_{fp}, and the Rayleigh number Ra will be reported. In addition, the effects of κ_{fp} and L on the change of the extreme dimensionless stream function $\Delta\psi$ and the maximum dimensionless temperature θ_{max} will be shown and analyzed. Furthermore, representative results for the local and average Nusselt numbers (i.e., Nu and $\overline{Nu}$) for various conditions will be presented and discussed. All results are computed for enclosure wall dimensionless thickness $\omega_e = 0.05$, enclosure wall thermal conductivity ratio $\kappa_e = 1$, fin dimensionless width $\omega_f = 0.01$, pipe dimensionless diameter $D = 0.2$, and pipe dimensionless thickness $\omega_p = 0.01$. The Prandtl number throughout the current study is set to 0.7 in accordance with the works of Acharya [4], Shim and Hyun [11] and Oztop and Bilgen [10] who employed the same Prandtl number value in their respective works on natural convection cavities with uniformly-distributed internal heat generation.

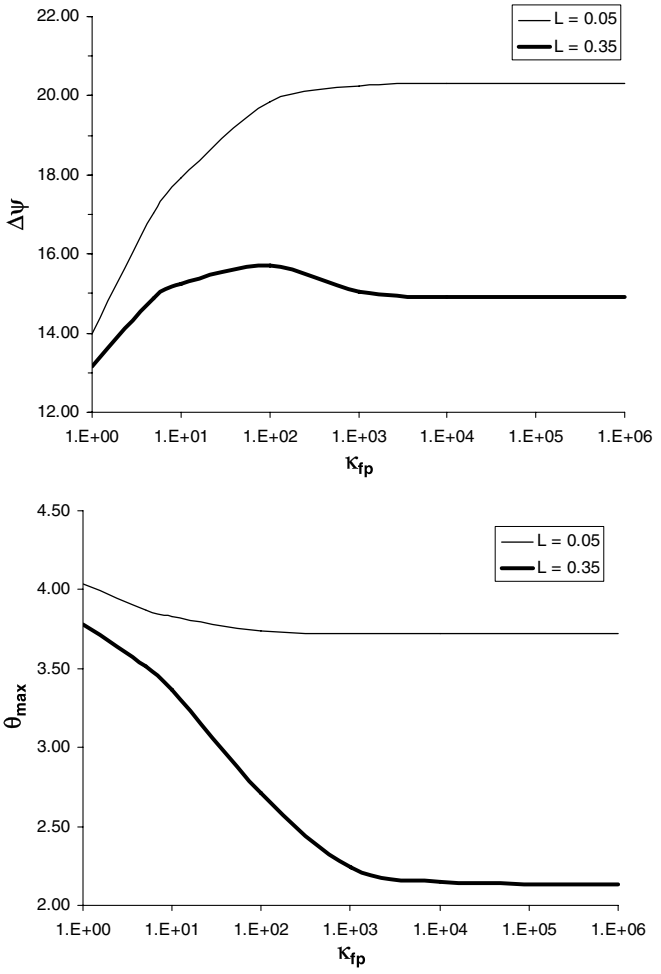

Fig. 6. Effects of κ_{fp} on $\Delta\psi$ and θ_{max} the for $\varepsilon = 0°$, $Ra_E = 10^5$, $Ra_I = 10^7$, and $L = 0.05$ and 0.35.

Fig. 5 presents steady-state contour plots for the streamline and temperature for various values of L and two values κ_{fp} (1 and ∞) at $\varepsilon = 0°$. The flow and thermal contours are symmetrical to the vertical centerline. The rise of the fluid due to buoyancy effects caused by internal heat generation and the consequent falling of the fluid on the enclosure walls and finned pipe surface creates multi-cellular vortices structure. It is observed that the addition of fins increases the cooling effect and that the maximum temperature decreases as the fin length increases. Furthermore, the strength of the relation between the finned pipe cooling effect and fin length is directly related to κ_{fp}. In other words, θ_{max} decreases as L increases at steeper rate for $\kappa_{fp} = \infty$ than that for $\kappa_{fp} = 1$. On the other hand, the presence of fins presents obstacle to the flow caused by the thermal buoyancy effect. The strength of the streamlines $\Delta\psi$ is related to L in a compound manner. While longer fins mean stronger obstruction to natural convection induced flow, increasing L increases the cooling effect (i.e. driving potential) and creates local vortices including less mass of fluid. In general, $\Delta\psi$ is inversely related to L for $\kappa_{fp} = 1$ and ∞ with an exception for $\kappa_{fp} = 1$ and $L = 0.2$.

The effects of κ_{fp} on the flow and temperature distribution for $L = 0.05$ and 0.35, $\varepsilon = 0°$, $Ra_E = 10^5$, and $Ra_I = 10^7$ was studied by monitoring $\Delta\psi$ and θ_{max} as shown in Fig. 6. In general, the values of $\Delta\psi$ increase while the values of θ_{max} decrease approaching asymptotic values as κ_{fp} increases. Clearly, both $\Delta\psi$ and θ_{max} have fixed values for $\kappa_{fp} \geqslant 10^3$ which is very common in heat exchangers. In addition, as mentioned before, both $\Delta\psi$ and θ_{max} decrease as the fin length L increases. For $L = 0.35$, it is observed that $\Delta\psi$ increases reaching a maximum at $\kappa_{fp} = 10^2$ and then decreases to approach the corresponding asymptotic value as κ_{fp} is increased further.

The effects of ε on the contour maps of the streamlines and isotherms for $L = 0.2$, $\kappa_{fp} = \infty$, $Ra_E = 10^5$, and $Ra_I = 10^7$ are presented in Fig. 7. It is observed that the

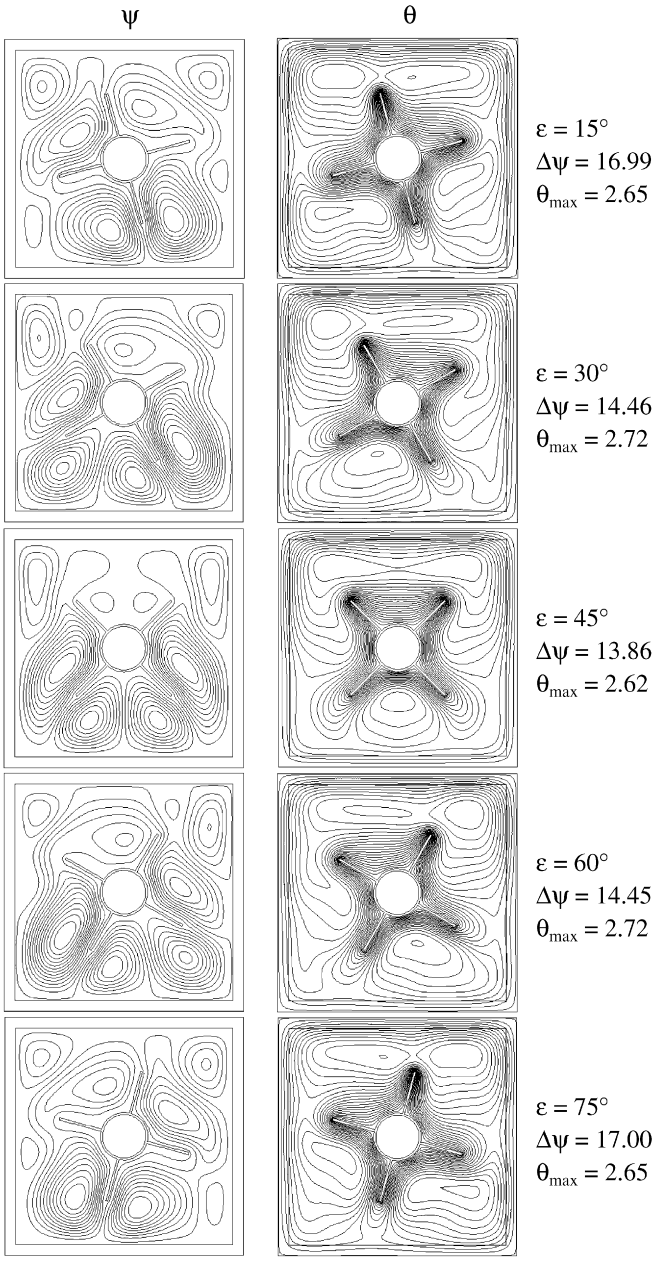

Fig. 7. Effects of ε on the contour maps of the streamlines and isotherms for $\kappa_{fp} = \infty$, $Ra_E = 10^5$, $Ra_I = 10^7$, and $L = 0.20$.

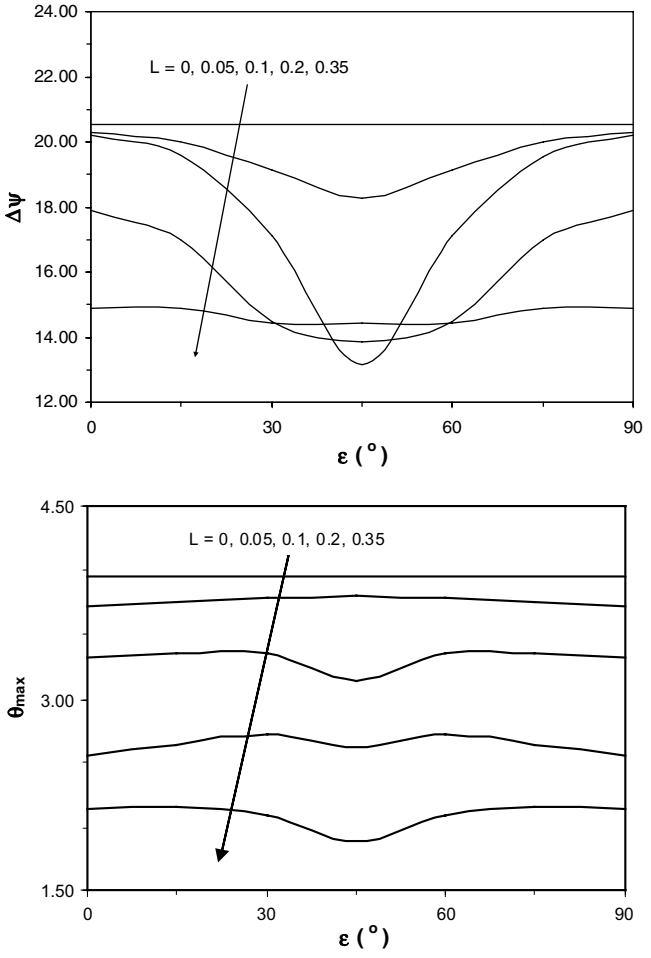

Fig. 8. Effects of ε on $\Delta\psi$ and θ_{max} for $\kappa_{fp} = \infty$, $Ra_E = 10^5$, $Ra_I = 10^7$, and different values of L.

flow streamlines show a complex interacting multi-cellular phenomenon as ε is increased. In addition, the contour plots for the streamlines and isotherms for $\varepsilon = 15°$ are the mirror images of those corresponding to $\varepsilon = 75°$ with respect to a vertical side of the enclosure. A similar relation exists between the contours plots for $\varepsilon = 30°$ and $\varepsilon = 60°$ while the contour maps for $\varepsilon = 45°$ are symmetrical with respect to the vertical centerline.

Fig. 8 depicts the changes in the values of $\Delta\psi$ and θ_{max} that are brought about by changing the values of ε and L. As shown by this figure, the values of $\Delta\psi$ decrease from $\varepsilon = 0°$ to $\varepsilon = 45°$ and then increase in a mirror way from $\varepsilon = 45°$ to $\varepsilon = 90°$ (i.e. $\varepsilon = 0°$). The profiles of θ_{max} are also symmetrical with respect to θ_{max} value at $\varepsilon = 45°$. For $L = 0.05$ the peak value of θ_{max} occurs at $\varepsilon = 45°$, while for the remaining profiles of θ_{max} the peak value of θ_{max} occurs at $\varepsilon = 30°$ and 60° with the minimum value of θ_{max} occurring at $\varepsilon = 45°$.

The heat transfer behavior in the enclosure under consideration can be explored by the heat flux distributions on the solid–fluid interface. For the current domain two solid–fluid interfaces can be distinguished: the interface between the enclosure walls and the fluid, and the interface between the finned pipe and the fluid. While it is usually desired to increase heat flow (i.e. Nusselt number) at the latter interface, different targets are possible for the heat transfer between the fluid and enclosure walls. In fact, for some applications, the required category for heat flow across the enclosure wall–fluid interface may be dependent on the direction of heat flow.

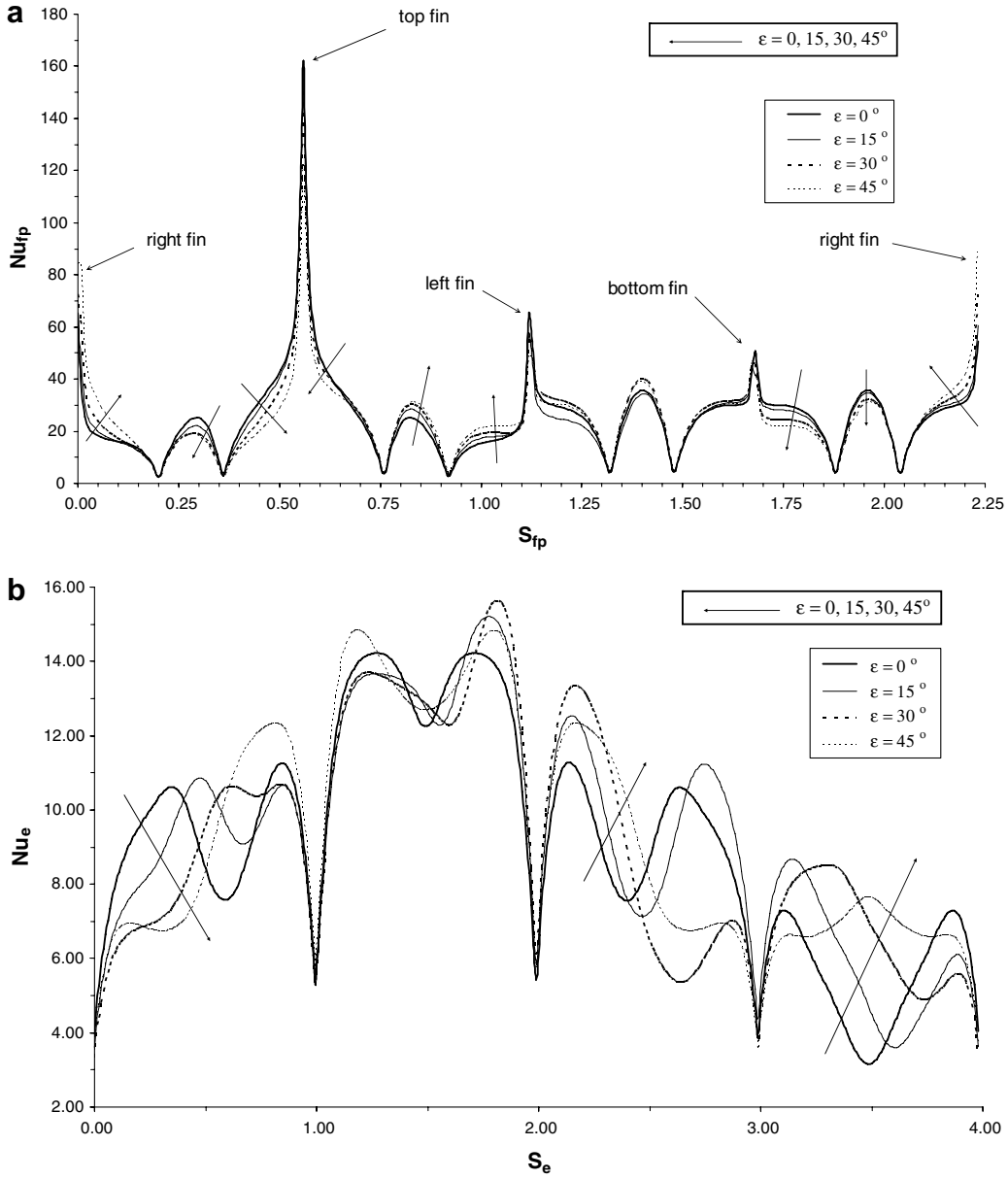

Fig. 9. Effects of ε on Nu_{fp} and Nu_e for $L = 0.20$, $\kappa = \infty$, $Ra_E = 10^5$, and $Ra_I = 10^7$.

The heat transfer behavior in the enclosure under consideration can be explored by the heat flux distributions on the solid–fluid interfaces. Fig. 9 presents the local Nusselt number Nu profiles at the finned pipe interface with the cavity Nu_{fp} and at the enclosure wall–cavity interface Nu_e for $L = 0.20$, $\kappa = \infty$, $Ra_E = 10^5$, $Ra_I = 10^7$, and different values of ε. For clarity, Nu profiles for $\varepsilon = 60°$ and 75° are not included in the figure as they can be predicted directly from Nu profiles for $\varepsilon = 30°$ and 15°, respectively, due to the symmetrical behavior shown in Fig. 7 between each couple of angles. The Nu_{fp} profiles start at the upper tip of the right fin, while the Nu_e profiles start from the lower right corner of the cavity as shown in Fig. 1 and all profiles are in counter-clockwise direction. The fin segments can be easily distinguished from the Nu_{fp} profiles, and the enclosure edges can also be recognized from the Nu_e profiles. For $\varepsilon = 0°$, the Nu_{fp} profile is symmetrical with respect to the centerline passing through the upper and lower fins. This is in accordance with the symmetrical contour maps of the streamlines and isotherms for $\varepsilon = 0°$ shown in Fig. 5. The relative position of the Nu_{fp} profiles is indicated by the arrows showing the order of the profiles in ascending sorting. In general, the upper the segment of the finned pipe (i.e. fin or pipe section), the higher the Nu_{fp} value. Hence, when ε causes the rising of a segment, its associated Nu_{fp} value usually increases and visa versa. The exception is when ε causes better local fluid flow, such as the case at the pipe sector between the left and bottom fins where the local Nu_{fp} value is maximum at $\varepsilon = 30°$ then $\varepsilon = 45°$, 0°, and 15°. On the other hand, the Nu_e profile for $\varepsilon = 0°$ is symmetrical with respect to $S_e = 1.5$ or 3.5 as indicated in Fig. 5. Furthermore, the Nu_e value is strongly related to ε as can be depicted from the various Nu_e profiles presented.

The effects of L and ε on the average Nusselt number $\overline{Nu}$ at the solid–fluid interfaces are illustrated in Fig. 10. Three values of $\overline{Nu}$ are monitored: the value of $\overline{Nu}$ at the enclosure wall–cavity interface $\overline{Nu}_e$, the value of $\overline{Nu}$ at the finned pipe–cavity interface $\overline{Nu}_{fp}$, and the value of $\overline{Nu}$ at the internal surface of the finned pipe $\overline{Nu}_{in}$. The dependence of $\overline{Nu}$ on L is stronger than that on ε for the three monitored boundaries. Furthermore, increasing the value of L reduces the heat flow rate between the cavity and outside (i.e. $\overline{Nu}_e$) and intensifies the heat flow rate between the cavity and the fluid inside the pipe (i.e. $\overline{Nu}_{in}$). Despite that for steady state

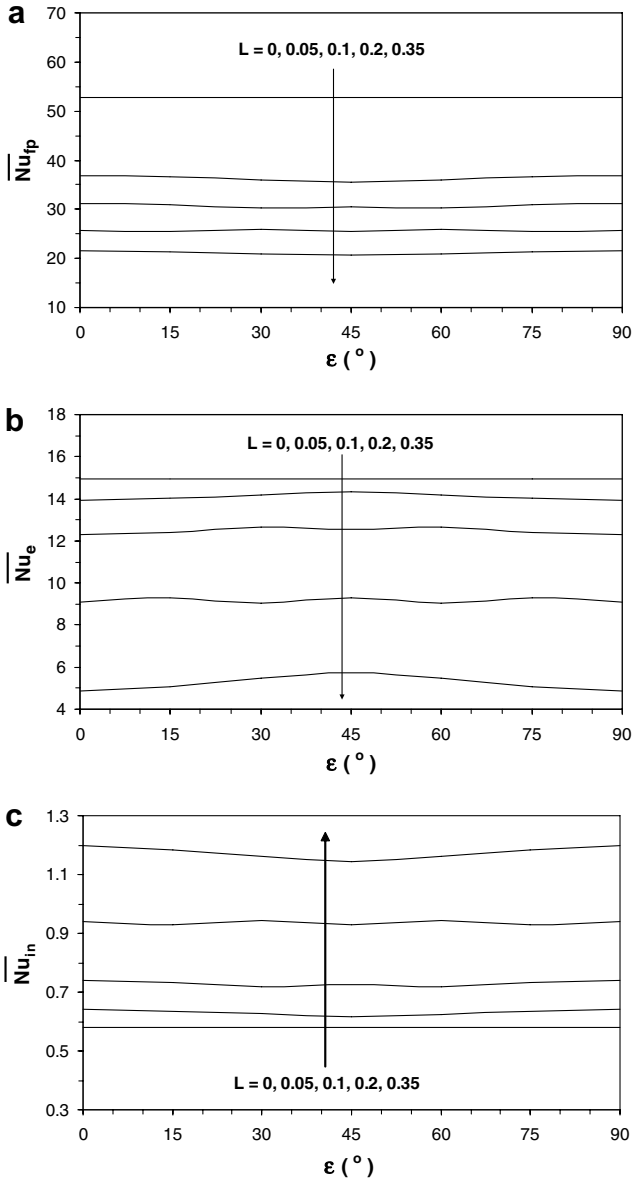

Fig. 10. Effects of ε and L on (a) Nu_{fp}, (b) Nu_e, and (c) Nu_{in}, for $\kappa = \infty$, $Ra_E = 10^5$, and $Ra_I = 10^7$.

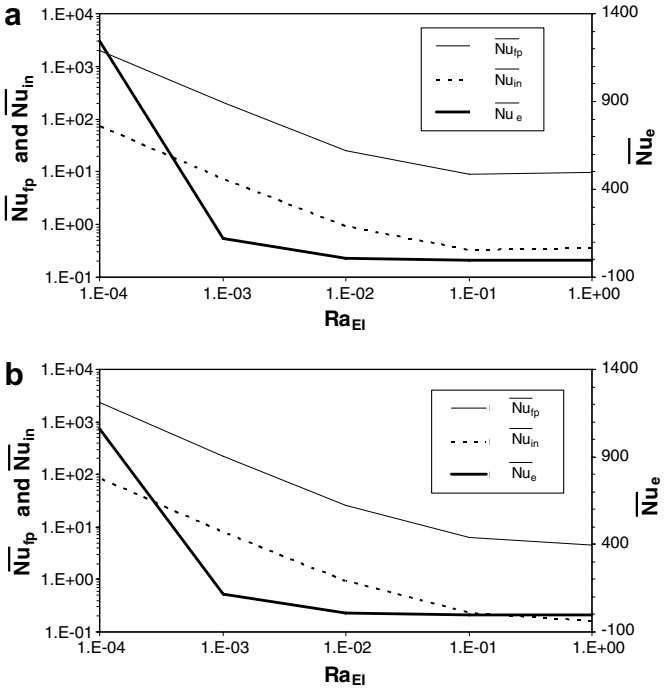

Fig. 11. Dependence of Nu_{fp}, Nu_e, and Nu_{in} on (a) Ra_E ($Ra_I = 10^7$) and (b) Ra_I ($Ra_E = 10^5$), for $\kappa = \infty$, $\varepsilon = 45°$ and $L = 0.2$.

results $\int_0^Z (\partial\theta/\partial N_{\mathrm{fp}})_{N_{\mathrm{fp}}=0}\,\mathrm{d}S_{\mathrm{fp}} = \int_0^{\pi D} (\partial\theta/\partial \mathrm{N}_{\mathrm{in}})_{N_{\mathrm{in}}=0}\,\mathrm{d}S_{\mathrm{in}}$, the $\overline{Nu}_{\mathrm{fp}}$ response to an increase in L is contrary to the response of $\overline{Nu}_{\mathrm{in}}$. This is because $1/\pi D$ is independent of L, while as L increases, $1/Z$ decreases faster than the rise in $\int_0^Z (\partial\theta/\partial \mathrm{N}_{\mathrm{fp}})_{N_{\mathrm{fp}}=0}\mathrm{d}S_{\mathrm{fp}}$. This explains why $\overline{Nu}_{\mathrm{fp}}$ and $\overline{Nu}_{\mathrm{in}}$ are inversely and directly related to L, respectively.

Finally, Fig. 11 depicts the influence of the external to internal Rayleigh numbers ratio (i.e. $Ra_{\mathrm{EI}} = Ra_{\mathrm{E}}/Ra_{\mathrm{I}}$) on the three average Nusselt numbers (i.e. $\overline{Nu}_{\mathrm{fp}}$, $\overline{Nu}_{\mathrm{e}}$, and $\overline{Nu}_{\mathrm{in}}$) for $\kappa = \infty$, $\varepsilon = 45°$ and $L = 0.2$. In Fig. 11a, Ra_{I} was fixed at 10^7 and Ra_{E} was varied from 10^3 to 10^7. However, in Fig. 11b, Ra_{E} was assigned to 10^5 and Ra_{I} was varied from 10^5 to 10^9. By inspecting Eq. (4), one observes that increasing the ratio Ra_{EI} results in reductions in the heat generation effect and vice versa. This should be considered in interpreting the effects of Ra_{EI} on $\overline{Nu}_{\mathrm{fp}}$, $\overline{Nu}_{\mathrm{e}}$ and $\overline{Nu}_{\mathrm{in}}$. It is clearly seen from these figures that as the ratio Ra_{EI} increases, all of $\overline{Nu}_{\mathrm{fp}}$, $\overline{Nu}_{\mathrm{e}}$ and $\overline{Nu}_{\mathrm{in}}$ decrease each approaching asymptotically a fixed value at $Ra_{\mathrm{EI}} = 1$. Since L is constant, the ratio between $\overline{Nu}_{\mathrm{fp}}$ and $\overline{Nu}_{\mathrm{in}}$ is constant in both figures, and both change at similar rates with increases in the value of Ra_{EI}. However, although the trend of $\overline{Nu}_{\mathrm{e}}$ is similar to those of $\overline{Nu}_{\mathrm{fp}}$ and $\overline{Nu}_{\mathrm{in}}$ as mentioned above, its rate of decrease as Ra_{EI} increases is much faster and the asymptotic value is reached at $Ra_{\mathrm{EI}} = 0.01$ and higher.

5. Conclusions

Conjugate natural convection heat transfer in a square enclosure having thick walls and encompasses a finned pipe at its center was studied numerically. The governing equations for this investigation were put in the dimensionless formulation and were solved by the finite-volume technique. Graphical results for the streamline and temperature contours for several parametric conditions were presented and discussed. It is concluded that the maximum temperature and extreme stream function difference can be controlled through the finned pipe inclination angle and fins length. It was also found that the finned pipe inclination angle, fins length, and external and internal Rayleigh numbers have significant effects on the local and average Nusselt number at the enclosure wall-cavity and finned pipe–cavity interfaces. The presence of fins had two different effects, restraining the fluid flow and increasing the heat transfer rate through the cavity and its surrounding solid–fluid interfaces. Therefore, in design applications, it is possible to control heat transfer between the cavity and its surrounding boundary by proper selection of both finned pipe inclination angle and fins length based on the associated Prandtl number, the enclosure wall thickness and thermal conductivity, fin width and thermal conductivity, pipe diameter, pipe thickness and thermal conductivity, and internal and external Rayleigh numbers.

Acknowledgements

The authors wish to express their appreciation for the support from the Public Authority for Applied Education and Training, Kuwait.

References

[1] U. Steinberner, H.H. Reinke, Turbulent buoyancy convection heat transfer with internal heat source, Sixth International Heat Transfer Conference, Toronto, Canada, August 7–11, vol. 2, Hemisphere Publishing Corp., Washington, DC, 1978, NC-21, pp. 305–311.
[2] F.A. Kulacki, R.J. Goldstein, Thermal convection in a horizontal fluid layer with uniform volumetric energy sources, J. Fluid Mech. 55 (Pt. 2) (1972) 271–287.
[3] J.H. Lee, R.J. Goldstein, An experimental study on natural convection heat transfer in an inclined square enclosure containing internal energy sources, ASME J. Heat Transfer 110 (1988) 345–349.
[4] S. Acharya, R.J. Goldstein, Natural convection in an externally heated vertical or inclined square box containing internal energy sources, ASME J. Heat Transfer 107 (1985) 855–866.
[5] A.A. Emara, F.A. Kulacki, A numerical investigation of thermal convection in a heat-generating fluid layer, ASME J. Heat Transfer 102 (1980) 531–537.
[6] M. Rahman, M.A.R. Sharif, Numerical study of laminar natural convection in inclined rectangular enclosures of various aspect ratios, Numer. Heat Transfer A 44 (2003) 355–373.
[7] Z. Kawara, I. Kishiguchi, N. Aoki, I. Michiyoshi, Natural convection in a vertical fluid layer with internal heating. In: Proceedings of the 27th National Heat Transfer Symposium, Japan, vol. II, 1990, pp. 115–117.
[8] T. Fusegi, J.M. Hyun, K. Kuwahara, Natural convection in a differentially heated square cavity with internal heat generation, Numer. Heat Transfer A 21 (1992) 215–229.
[9] T. Fusegi, J.M. Hyun, K. Kuwahara, Numerical study of natural convection in a differentially heated cavity with internal heat generation: effects of the aspect ratio, J. Heat Transfer 114 (1992) 773–777.
[10] H. Oztop, E. Bilgen, Natural convection in differentially heated and partially divided square cavities with internal heat generation, Int. J. Heat Fluid Flow (2006).
[11] Y.M. Shim, J.M. Hyun, Transient confined natural convection with internal heat generation, Int. J. Heat Fluid Flow 18 (1997) 328–333.
[12] A.C. Baytas, Buoyancy-driven flow in an enclosure containing time periodic internal sources, Heat Mass Transfer 31 (1996) 113–119.
[13] A. Liaqat, A.C. Baytas, Conjugate natural convection in a square enclosure containing volumetric sources, Int. J. Heat Mass Transfer 44 (2001) 3273–3280.
[14] S.V. Patankar, Numerical Heat Transfer and Fluid Flow, Hemisphere Publishing Corp., Washington, DC, 1980.
[15] J.P. Vandoormaal, G.D. Raithby, Enhancements of the Simple Method for Predicting Incompressible Fluid Flows, Numerical Heat Transfer 7 (1984) 147–163.
[16] D.A. Kaminski, C. Prakash, Conjugate natural convection in a square enclosure: effect of conduction in one of the vertical walls, Int. J. Heat Mass Transfer 29 (1986) 1979–1988.
[17] A. Ben-Nakhi, A. Chamkha, Conjugate natural convection in a square enclosure with inclined thin fin of arbitrary length, Int. J. Therm. Sci., accepted for publication.
[18] S. Dong, Y. Li, Conjugate of natural convection and conduction in a complicated enclosure, Int. J. Heat Mass Transfer 47 (2004) 2233–2239.